# Laplacian eigenmodes in twisted periodic topologies for new physics models

**Anele Ncube**[1,2], **Aldo Deandrea**[2,1], **Alan S. Cornell**[1] **and Rhameez S. Herbst**[3]

[1] Department of Physics, University of Johannesburg, PO Box 524, Auckland Park 2006, South Africa.
[2] Université Claude Bernard Lyon 1, CNRS/IN2P3, IP2I UMR 5822, 4 Rue Enrico Fermi, F-69100 Villeurbanne, France.
[3] Department of Mathematics and Applied Mathematics, University of Johannesburg, PO Box 524, Auckland Park 2006, South Africa.

E-mail: ancube@uj.ac.za

**Abstract.** Laplacian eigenmodes in non-trivial topologies (e.g. having twisted periodicity) are important in constructing a complete picture of the physics at play within models that incorporate compact extradimensional spaces. Determining them analytically is generally unwieldy, and the existing standard numerical methods have limited ability as spatial dimensions increase and when computing higher-index eigenmodes is required. To determine the feasibility of using physics-informed neural networks to compute Laplacian eigenmodes, we apply them to three primitive test cases: the Möbius strip, the real projective plane ($\mathbb{R}P_2$) and the 3-torus ($\mathbb{T}_3$) in Cartesian coordinates. The potential performance of the neural networks approach beyond solving the simpler cases is estimated in terms of the approximation errors obtained by comparing them with known analytical solutions.

## 1 Introduction

The reduction of extra dimensions (i.e. compactification) is a crucial route for achieving the phenomenology of new physics in extra dimensions [1]. Compactification has its roots in seminal works, such as Ref. [2], where masses were generated in 4D space-time induced by higher-dimensional supergravity [3]. Subsequently, further realisations of compactification have considered, to a greater extent, extradimensional spaces with flat metrics, and, to a lesser extent, those with curved metrics, though phenomenologically the latter provide more interesting properties. For example, curved spaces give rise to a potential for specific 4D scalar fields, which gives them masses not arising otherwise [1]. Among negatively curved spaces, a special case is the nilmanifold, a manifold that has found use as a compactification scheme for Type II string theories and M theory, e.g. see Refs. [4, 5].

An $n$-nilmanifold (here $n$ denotes the number of spatial dimensions) is a smooth manifold $\mathcal{M}_n$ obtained by quotienting a nilpotent Lie group $A$ by a discrete subgroup $\Gamma$, i.e. $\mathcal{M}_n = A/\Gamma$. In general, Lie groups can be viewed as $n$-dimensional manifolds [6]. For the 3-nilmanifold, the Lie group of concern is the Weyl group, which is the only solvable Lie group in 3D [3]. Given that the associated Lie algebra is the Heisenberg algebra, $\mathcal{M}_3$ is otherwise known as the Heisenberg nilmanifold. For the Heisenberg algebra:

$$[V_1, V_2] = -\mathtt{f} V_3, \quad [V_1, V_3] = [V_2, V_3] = 0, \tag{1}$$

where $\mathtt{f}$ is a structure constant, the terms $V_{a=1,2,3}$ are contravariant vectors from which Maurer-Cartan one-forms $e^{a=1,2,3}$ (i.e. covariant vectors) can be determined [3]. The $V_a$ and $e^a$ terms form the basis of the (co)-tangent space of $\mathcal{M}_3$ whose metric in terms of the one-forms is [6]:

$$ds^2 = (e^1 + ae^3)^2 + (e^2 + be^3) + c^2(e^3)^2; a, b \in \mathbb{R}, \tag{2}$$

where $c$ is not a true parameter and can be set to unity without loss of generality.

$\mathcal{M}_3$ is parameterised by dimensionless angular coordinates $x^{m=1,2,3} \in [0, 1]$ related to the Maurer-Cartan one-forms according to [1, 6]:

$$e^1 = r^1 dx^1; \quad e^2 = r^2 dx^2; \quad e^3 = r^3(dx^3 + Nx^1 dx^2); \quad N = \frac{r^1 r^2}{r^3}\mathtt{f} \in \mathbb{Z}^*, \tag{3}$$

with $r^{m=1,2,3}$ being radii (they have units of length same as $e^{m=1,2,3}$). The topology of $\mathcal{M}_3$ is represented by discrete (or "twist") identifications describing how a unit cube, with $x^{m=1,2,3}$ as coordinates, is deformed via the joining of points on opposite faces to construct this space. They are the following:

$$(x^1, x^2, x^3) \sim (x^1, x^2 + 1, x^3) \sim (x^1, x^2, x^3 + 1) \sim (x^1 + 1, x^2, x^3 - Nx^2). \tag{4}$$

These identifications lead to the interpretation of $\mathcal{M}_3$ as a twisted fibration over a circle (in other words, a 2-torus in the $x^2$ and $x^3$ directions with changing geometry along the base circle parameterised by $x^3$, the fibre coordinate) [3, 6]. As such, $\mathcal{M}_3$ may be thought of as a twisted torus, a concept that can be applied in more general terms to nilmanifolds with spatial dimensions higher than $n = 3$.

The Laplacian on $\mathcal{M}_3$ has been used as a tractable example to construct the phenomenology of fields for toy models (e.g. scalars [6], gauge bosons [1] and spinors [7]) in extra dimensions. Mathematically, we have at hand a Sturm-Liouville problem that can be solved analytically, giving closed-form expressions for the associated eigenvalue spectrum. Concerning the physical significance of the solutions, the eigenvalues of the Laplacian correspond to masses, and the eigenfunctions provide a natural expansion basis for fields in extra dimensions. For more detailed models of negatively curved spaces, numerical analysis becomes necessary; however, many standard approaches are limited by the non-trivial and convoluted nature of the spaces involved.

This work has focused on testing physics-informed neural networks (PINNs) as a new numerical approach to the Laplacian on non-trivial topologies, beginning with calculable cases in $n = 2$ and 3 dimensional spaces with flat metrics. Ultimately, the aim is to test PINNs on the Laplacian on $\mathcal{M}_3$, which is not flat. Therefore, Section 2 will review the Laplacian on various spaces, starting with the relatively simple (i.e. the Möbius strip and real projective plane both in 2D space, and the 3-torus in 3D) and building up to the not so simple case of $\mathcal{M}_3$. Results of numerical analysis (using PINNs) of the Laplacian on each of these spaces are given in Section 3, where the performance of the PINN approach is reported in terms of relative mean square errors. Finally, discussions on the advantages of PINNs and their potential applicability in more challenging, less tractable extradimensional cases are discussed in the last section (Section 4).

## 2 Theory

To explore the Laplacian on $\mathcal{M}_3$ using numerical analysis, it is natural to first consider related spaces that represent simple building blocks by which $\mathcal{M}_3$ is constructed. These spaces are described, followed by the expressions of their eigenvalue spectra. Thereafter, the eigenvalues expected from $\mathcal{M}_3$ are given. Note that, in general, the Laplacian of a scalar field is:

$$\nabla^2\Phi = \frac{1}{\sqrt{g}}\partial_m(\sqrt{g}g^{mn}\partial_n\Phi), \tag{5}$$

where $g_{mn}$ is the metric for our flat-space Möbius strip, $\mathbb{R}P_2$ and $\mathbb{T}_3$, with $m, n = 1, 2, 3$. Therefore, the Laplacian is simply:

$$\nabla^2\Phi = (\partial_1^2 + \partial_2^2 + \partial_3^2)\Phi. \tag{6}$$

Setting $a = b = 0, c = 1$; $r^1 = r^2 = r^3 = 1$ and $\mathtt{f} = 1$, the metric of $\mathcal{M}_3$ (i.e. Equation 2) has components [6]:

$$g_{11} = 1; \quad g_{22} = 1; \quad g_{23} = g_{32} = 1; \quad g_{33} = 1 + x^2, \tag{7}$$

where $g = 1$ and the Laplacian is given as:

$$\nabla^2\Phi = (\partial_1^2 + (\partial_2 - x^1\partial_3)^2 + \partial_3^2)\Phi. \tag{8}$$

Imposing the relevant topology-based boundary conditions (i.e. discrete identifications), Equations (6) and (8) can be solved analytically using the method of separation of variables for the former and the Hermite differential

equation for the latter. While Equation (4) dictates the twisted periodic boundary conditions for $\mathcal{M}_3$, the relevant identifications for the simpler spaces are:

$$\text{Möbius strip:} \quad (x^1, x^2) \sim (x^1 + 1, -x^2), \quad x^{m=1,2} \in [-0.5, 0.5]^2; \tag{9}$$

$$\mathbb{R}P_2: \quad (x^1, x^2) \sim (x^1 + 1, -x^2) \sim (-x^1, x^2 + 1), \quad x^{m=1,2} \in [-0.5, 0.5]^2; \tag{10}$$

$$\mathbb{T}_3: \quad (x^1, x^2, x^3) \sim (x^1, x^2 + 1, x^3) \sim (x^1 + 1, x^2, x^3) \sim (x^1, x^2, x^3 + 1), \quad x^{m=1,2,3} \in [0, 1]^3. \tag{11}$$

For the Möbius strip, apart from the periodic boundary condition, there is a Dirichlet boundary condition; namely: $\Phi(x^1, 0.5) = \Phi(x^1, -0.5) = 0$. The corresponding eigenvalue spectra are [6, 8, 9]:

$$\text{Möbius strip:} \quad \lambda^2_{n_1,n_2} \supset \left\{\pi^2 \left(n_1^2 + n_2^2\right)\right\}_{\substack{n_1 \in \mathbb{Z}; n_2 \in \mathbb{N}\setminus\{0\} \\ n_1+n_2 \text{ odd}}}, \tag{12}$$

$$\mathbb{R}P_2: \quad \lambda^2_{n_1,n_2} \supset \left\{\pi^2 \left(n_1^2 + n_2^2\right)\right\}_{n_1,n_2 \in \mathbb{Z},} \tag{13}$$

$$\mathbb{T}_3: \quad \lambda^2_{n_1,n_2,n_3} \supset \left\{4\pi^2 \left(n_1^2 + n_2^2 + n_3^2\right)\right\}_{n_1,n_2,n_3 \in \mathbb{Z}}. \tag{14}$$

Note the two-fold and three-fold degeneracies in the 2D and 3D cases, respectively. The corresponding eigenfunctions can be found in Refs. [6, 9]. For $\mathcal{M}_3$ there are two families of eigenstates; namely, $\mathbb{T}_2$ modes satisfying the $x^3$ independent form of Equation (8) and fibre modes satisfying the $x^3$ dependent Laplacian. In this case, we have:

$$\mathbb{T}_2: \quad \mu^2_{p,q} \supset \left\{4\pi^2 \left(p^2 + q^2\right)\right\}_{p,q \in \mathbb{Z}}, \tag{15}$$

$$\mathcal{M}_3: \quad M^2_{n,k,\ell} \supset \left\{(2\pi k)^2 \left(1 + \frac{2n+1}{2\pi|k|}\right)\right\}_{k \in \mathbb{Z}\setminus\{0\}, n \in \mathbb{N}}, \tag{16}$$

where the $\ell$ index, not appearing in Equation (16), but appearing in the associated eigenfunctions implies degeneracy of level $|k|$, since $0 \leq \ell \leq |k| - 1$. Importantly, note that the associated eigenfunctions on $\mathcal{M}_3$ are non-separable in the coordinates $x^{m=1,2,3}$, unlike the associated eigenfunctions on the other simpler spaces. Both Equations (15) and (16) form complete sets of eigenvalues whose corresponding eigenmodes can naturally serve as expansion bases for fields in higher-dimensional spaces. Note also that the eigenvalues scale with the sizes of the spaces and the specific forms given are relevent for the specified radii and lengths for the sides of the deformed unit squares and unit cubes.

## 3 Numerical analysis

Knowing the exact solutions of the Laplacian on some example 2D and 3D spaces, numerical methods like PINNs can be tested, allowing us to infer their potential performance in problems that are non-trivial, not easily calculable (due to the negative spatial curvature). Some of the calculable cases also provide physically interesting properties, which make them, in their own right, worth studying.

### *3.1 Principle of the analysis*

Using PINNs, we begin with an ansatz consisting of many tunable parameters to be updated based on the evaluation of the Laplacian and the relevant boundary conditions at selected points (i.e. the unlabelled training points). Since no approximation is required to numerically evaluate the derivatives like mesh-based methods (e.g. using the Cornish & Turok approach [10]), the contribution of truncation errors to numerical errors is alleviated. Given in Table 1 is the algorithm followed by the PINN approach, where note that the terms $w^\ell_{jk}$ and $b^\ell_j$ denote the tunable weights of the neural network (NN) ansatz $f(x_i)$ serving as the approximate solution to the differential equation. To facilitate the solving of a differential equation, the same is embedded in the loss function $\mathcal{L}$ that includes the physical constraints and extra terms that penalise $f(x_i) = 0$ and enforce the scanning of $\hat{E}$ in the positive direction. With the latter loss term, training over a set number of epochs encourages the learning of several $\hat{E}$ (note: an epoch consists of a single run through the entire training data). The total loss is given generically as:

$$\mathcal{L} = \mathcal{L}_{PDE} + \mathcal{L}_{BC} + \mathcal{L}_{\text{extra}}. \tag{17}$$

The loss terms $\mathcal{L}_{PDE}, \mathcal{L}_{BC}$ are mean square errors of the PDE (residual) and the boundary conditions; $\mathcal{L}_{\text{extra}}$ dynamically constrains $f(x_i, \theta)$ and $\hat{E}$. Specifically, $\mathcal{L}_{\text{extra}}$ is given as [11]:

$$\mathcal{L}_{\text{extra}} = \frac{1}{\|\hat{f}\|^2} + \frac{1}{\|\hat{E}\|^2} + \|e^{-\hat{E}_{\text{init}} + \hat{E}_{\text{step}}}]\|^2, \tag{18}$$

where the first two terms penalise the $f(x_i) = 0$ and $E = 0$ as solutions to the PDE. The third term enforces the learning of eigenvalues in ascending order as the NN runs through its training loop.

- Initialise $\hat{E} = 1$ and NN ansatz parameters $\theta = \left\{w_{jk}^{\ell}, b_j^{\ell}\right\}_{1\leq\ell\leq L}$ randomly from e.g. $U(-\sigma, \sigma)$.
- **For each** epoch **in** training epochs:
  1. **Input** $x_i$ (training points) + **Evaluate** $f(x_i, \theta)$ and $\mathcal{L}(\theta)$.
  2. **Backpropagate:** compute $\dfrac{\partial\mathcal{L}}{\partial\theta} = \left\{\dfrac{\partial\mathcal{L}}{\partial w_{jk}^{\ell}}, \dfrac{\partial\mathcal{L}}{\partial b_j^{\ell}}\right\}_{1\leq\ell\leq L}$ with automatic differentiation.
  3. **Update** $\theta$**:** according to your chosen gradient-based (hence the previous step) optimisation algorithm (e.g. ADAM is a standard optimiser) [12].
  4. **Increment** $\hat{E}$ after specified epochs (enforces search for eigenvalue near the new $\hat{E}$).

Table 1: The algorithm for optimising ansatz $f(x_i, \theta)$ by minimising $\mathcal{L}(\theta)$.

| Möbius strip | $\mathbb{R}P_2$ | $\mathbb{T}_3$ | $\mathcal{M}_3$ |
|---|---|---|---|
| | $E_n$ | | $\mu_{p,q}^2$ |
| $E_1$/2: 4.95 | $E_2$/2: 9.82 | $E_1$/2: 9.87 | $\mu_{0,1}^2$/2: 19.74 |
| (0.2928%) | (0.0225%) | (0.0426%) | (0.0265%) |
| $E_2$/2: 24.67 | $E_3$/2: 19.74 | $E_2$/2: 19.74 | $\mu_{1,1}^2$/2: 39.54 |
| (-0.004%) | (0.0094%) | (-0.0101%) | (0.1450%) |
| $E_4$/2: 64.15 | $E_4$/2: 24.81 | $E_3$/2: 29.62 | $\mu_{0,2}^2$/2: 78.87 |
| (-0.0087%) | (0.5597%) | (0.0320%) | (-0.1145%) |
| $E_5$/2: 83.87 | $E_5$/2: 39.48 | $E_4$/2: 39.46 | $\mu_{2,1}^2$/2: 99.33 |
| (-0.0233%) | (0.0018%) | (-0.0351%) | (0.6387%) |
| $E_7$/2: 143.11 | $E_8$/2: 64.15 | $E_5$/2: 49.34 | $\mu_{2,2}^2$/2: 158.04 |
| (-0.0028%) | (0.0008%) | (-0.0189%) | (0.0769%) |

Table 2: First five PINN approximated eigenvalues and their percentage errors.

### *3.2 Details of the implementation*

We used the PyTorch library in Python to implement PINNs in a mostly standard way, i.e. using a fully-connected neural network as the architecture, incorporating the PDE of interest in the loss function, and using the ADAM optimiser as our NN update algorithm. For the relatively simple 2D and 3D spaces, solved analytically by trigonometric functions, it was sufficient to use a single hidden-layer NN with input and output nodes dictated by the variables of the PDE. In general, training was carried out for at most $\sim 10^6$ epochs, with a learning rate of $\sim 10^{-1}$ and the number of training points set to $4^n$ for $n = 2$ or 3 dimensions of space. These are intentionally rough specifications because they are parameters that are not directly determined by the physics at hand. They are instead related to the optimisation algorithm and its optimal configuration in relation to the setup of other parts of the PINN, such as the architecture.

### *3.3 Results*

Table 2 and Figure 1 give the low-lying eigenvalues of the Laplacian on the 2D and 3D spaces of interest. Figure 1 is an example plot of the typical losses and approximations of the eigenvalues generated as training progresses. The tunable parameter representing the eigenvalue (initially set to one) converges on discrete points in eigenvalue space where the PINN loss is minimised. The losses are subsequently pushed out of the minima to scan for higher

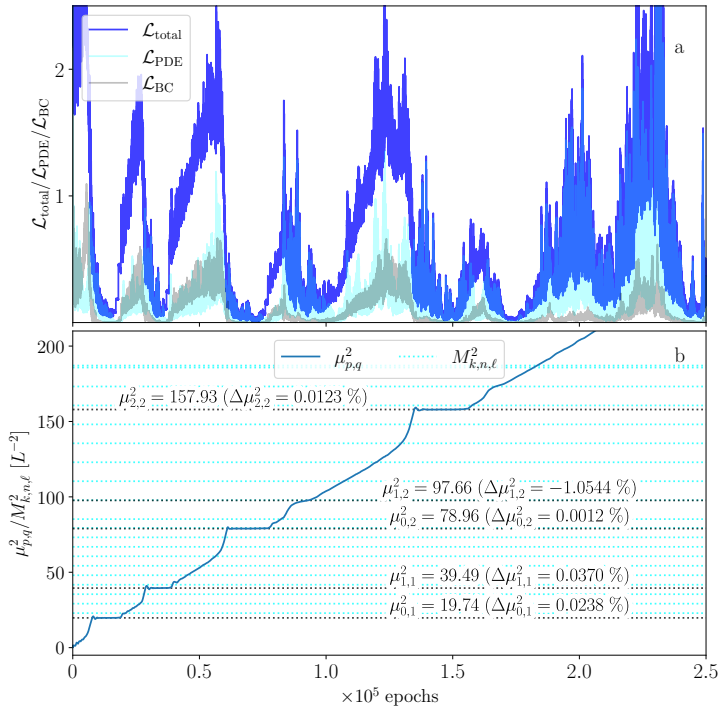


Figure 1: The PINN loss and approximations of $\mu^2_{p,q}$ given exactly by Equation 15.

eigenstates. The duration, in epochs, of convergence to a particular eigenvalue (seen as plateaus in the plot of the PINN approximate eigenvalues) is indirectly controlled by the $\hat{E}_{\text{step}}$ in the last loss term of Equation (18).

As can be inferred from Table 2, the Laplacian on twisted periodic manifolds is well approximated by our mainly standard PINN algorithm with the topology enforced as boundary conditions in the loss function as in Equation (17). For many of the identified eigenmodes, the accuracy of the approximations relative to the exact values is high (i.e. <1% relative mean square error). However, some eigenvalues (e.g. the $\mu^2_{1,2}$ approximation seen in Figure 1) have larger errors compared to others due to the algorithm spending less time minimising the loss (i.e. learning the eigenvalue) at those values. Partial control of the convergence duration can be achieved by tweaking the $\hat{E}_{\text{step}}$ (reducing it increases the duration, at the cost of reduced speed of adjustment of the eigenvalue parameter).

Given so far are the $\mathbb{T}_2$ modes of the Laplacian in $\mathcal{M}_3$. As can be seen in Figure 1, the $\mu^2_{p,q}$ eigenvalues are learned while the $M^2_{k,n,\ell}$ eigenvalues are not identified. There is, therefore, a limitation to the standard implementation of PINNs in the multivariable contexts where separation of variables occurs by default, making non-separable functions (such as the fibre modes) difficult to learn. What our results show is that twisted periodic topology is not, per se, a challenge for PINNs (nor is dimensionality). This point is borne out by our PINN's favorable performance considering the twisted periodic topology of the Möbius strip and $\mathbb{R}P_2$, and the high-dimensional case of $\mathbb{T}_3$. As such, there is a good chance to numerically determine $M^2_{k,n,\ell}$ for $\mathcal{M}_3$ given an effective modification to the PINN algorithm, currently under investigation.

## 4 Discussions and Conclusions

This work sought to test a recently developed numerical method based on artificial neural networks [13] in the context of particle physics phenomenology on compactified extradimensional spaces. The task at hand was to solve the Laplacian on the 3-nilmanifold, a space whose topology can be thought of as consisting of several compounding aspects; namely, three spatial dimensions, non-trivial topology, and negatively curved geometry. Since the Möbius strip, $\mathbb{R}P_2$, and $\mathbb{T}_3$ capture these aspects separately, they were naturally the first test cases considered. The accuracy remained comparable across different numbers of dimensions and boundary conditions considered, implying PINNs adapt well in various scenarios. We can attribute this to the use of automatic differentiation in lieu of numerical differentiation, an approach that facilitates exact evaluation of gradients and, as such, avoids the truncation errors of other numerical methods.

Our standard PINN approach runs into challenges when applied to $\mathcal{M}_3$ because the optimisation algorithm favours removing $x^3$ dependence, such that the problem being solved is the Laplacian on $\mathbb{T}_2$ with eigenvalues $\mu^2_{p,q}$. This is a simpler problem to solve, not only because of the reduced dimensionality and relatively more trivial periodic boundary conditions, but also because the solution functions are separable (the fibre modes are not). Alleviating this challenge requires enforcing the learning of non-separable functions in problems simultaneously satisfied by two or more families of linearly independent solutions (like we see with the Laplacian on $\mathcal{M}_3$).

Future work will continue to look at twisted periodic topologies, but with more focus on curved geometry, such as the curved Möbius strip that has been studied extensively within the literature using traditional numerical techniques [8, 9]. A more rigorous comparison between PINNs and other established techniques would be worth conducting to determine, more clearly, the advantages of the former. In terms of physically significant problems, the PINN approach could be applied in less calculable cases such as those involving gauge fields and fermions (no localised fields); the direction followed by Ref. [6].

**Acknowledgements**
ASC is supported in part by the National Research Foundation (NRF) of South Africa; AMN is supported by iThemba LABS and Campus France.

**References**

[1] D. Andriot and D. Tsimpis, "Laplacian spectrum on a nilmanifold, truncations and effective theories," *J. High Energy Phys.*, vol. 2018, p. 96, 2018.

[2] J. Scherk and J. H. Schwarz, "How to get masses from extra dimensions," *Nucl. Phys. B*, vol. 153, pp. 61–88, 1979. [Online]. Available: https://www.sciencedirect.com/science/article/pii/0550321379905923

[3] A. Chatzistavrakidis and L. Jonke, "Matrix theory compactifications on twisted tori," *Phys. Rev. D*, vol. 85, p. 106013, May 2012. [Online]. Available: https://link.aps.org/doi/10.1103/PhysRevD.85.106013

[4] S. Kachru, M. B. Schulz, P. K. Tripathy, and S. P. Trivedi, "New supersymmetric string compactifications," *J. High Energy Phys.*, vol. 2003, no. 03, p. 061, apr 2003. [Online]. Available: https://dx.doi.org/10.1088/1126-6708/2003/03/061

[5] C. Hull and R. Reid-Edwards, "Flux compactifications of string theory on twisted tori," *Fortschr. Phys.*, vol. 57, no. 9, pp. 862–894, 2009. [Online]. Available: https://onlinelibrary.wiley.com/doi/abs/10.1002/prop.200900076

[6] D. Andriot, G. Cacciapaglia, A. Deandrea, N. Deutschmann, and D. Tsimpis, "Towards kaluza-klein dark matter on nilmanifolds," *J. High Energy Phys.*, vol. 2016, no. 6, p. 169, 6 2016. [Online]. Available: https://doi.org/10.1007/JHEP06(2016)169

[7] A. Deandrea, F. Dogliotti, and D. Tsimpis, "Dirac operator spectrum on a nilmanifold," *Nucl. Phys. B*, vol. 982, p. 115895, 2022.

[8] T. Kalvoda, D. Krejčiřík, and K. Zahradová, "Effective quantum dynamics on the möbius strip," *J. Phys. A: Math. Theor.*, vol. 53, no. 37, p. 375201, aug 2020. [Online]. Available: https://dx.doi.org/10.1088/1751-8121/ab8b3a

[9] Z. Li and L. R. Ram-Mohan, "Quantum mechanics on a möbius ring: Energy levels, symmetry, optical transitions, and level splitting in a magnetic field," *Phys. Rev. B*, vol. 85, p. 195438, May 2012. [Online]. Available: https://link.aps.org/doi/10.1103/PhysRevB.85.195438

[10] N. J. Cornish and N. G. Turok, "Ringing the eigenmodes from compact manifolds," *Class. Quantum Grav.*, vol. 15, no. 9, p. 2699, sep 1998. [Online]. Available: https://dx.doi.org/10.1088/0264-9381/15/9/016

[11] H. Jin, M. Mattheakis, and P. Protopapas, "Unsupervised neural networks for quantum eigenvalue problems," 2020. [Online]. Available: https://arxiv.org/abs/2010.05075

[12] D. P. Kingma and J. Ba, "Adam: A method for stochastic optimization," 2017. [Online]. Available: https://arxiv.org/abs/1412.6980

[13] M. Raissi, P. Perdikaris, and G. Karniadakis, "Physics-informed neural networks: A deep learning framework for solving forward and inverse problems involving nonlinear partial differential equations," *J. Comput. Phys.*, vol. 378, pp. 686–707, 2019. [Online]. Available: https://www.sciencedirect.com/science/article/pii/S0021999118307125